ISTITUTO DI ANALISI DEI SISTEMI ED INFORMATICA
CONSIGLIO NAZIONALE DELLE RICERCHE

A. Bertuzzi, A. Fasano, A. Gandolfi, D. Marangi

CELL KINETICS IN TUMOUR CORDS STUDIED BY A MODEL WITH VARIABLE CELL CYCLE LENGTH

R. 536 Novembre 2000

Alessandro Bertuzzi – Istituto di Analisi dei Sistemi ed Informatica del CNR, viale Manzoni 30 - 00185 Roma, Italy. Email : bertuzzi@iasi.rm.cnr.it.

Antonio Fasano – Dipartimento di Matematica "U. Dini", Università di Firenze, Viale Morgagni 67/A, 50134 Firenze, Italy Email : fasano@math.unifi.it.

Alberto Gandolfi – Istituto di Analisi dei Sistemi ed Informatica del CNR, viale Manzoni 30 - 00185 Roma, Italy. Email : gandolfi@iasi.rm.cnr.it.

Doriana Marangi – Present address: Ekar s.p.a., Via Terenzio 35, 00193 Roma, Italy..

ISSN: 1128–3378

Collana dei Rapporti
dell'Istituto di Analisi dei Sistemi ed Informatica, CNR

viale Manzoni 30, 00185 ROMA, Italy

tel. ++39-06-77161
fax ++39-06-7716461
email: iasi@iasi.rm.cnr.it
URL: http://www.iasi.rm.cnr.it

Abstract

A mathematical model is developed that describes the proliferative behaviour at the stationary state of the cell population within a tumour cord, i.e. in a cylindrical arrangement of tumour cells growing around a blood vessel and surrounded by necrosis. The model, that represents the tumour cord as a continuum, accounts for the migration of cells from the inner to the outer zone of the cord and describes the cell cycle by a sequence of maturity compartments plus a possible quiescent compartment. Cell-to-cell variability of cycle phase transit times and changes in the cell kinetic parameters within the cord, related to changes of the microenvironment, can be represented in the model. The theoretical predictions are compared against literature data of the time course of the labelling index (LI) and of the fraction of labelled mitoses (FLM) in an experimental tumour after pulse labelling with ^{3}H-thymidine. It is shown that the presence of cell migration within the cord can lead to a marked underestimation of the actual changes along cord radius of the kinetics of cell cycle progression.

Key words: Solid tumours; Cell migration; Cell kinetics; Mathematical model.

1. Introduction

According to a common view on tumour development, solid tumours start their growth as spheroids of proliferating cells that receive oxygen and nutrients necessary to survive and proliferate only through diffusion from the external environment, the neighbouring blood vessels running externally to the tumour. This avascular phase is followed by angiogenesis, stimulated by factors released by tumour hypoxic cells, to develop a vascular network inside the tumour mass itself, that supports its further growth [1]. Experimental models of the avascular phase of tumour growth are the multicellular spheroids grown *in vitro* [2]. The growth of multicellular spheroids or of solid tumours in their initial avascular phase, up to 1–2 mm in diameter, has been investigated by mathematical models (see the review in [3]).

The above view seems to be quite adequate for the initial growth of experimental tumours implanted subcutaneously, because tumour cells are placed in a space that is devoid of vessels, thus requiring angiogenesis to provide vessels to the tumour. For spontaneous tumours or experimental tumours implanted not subcutaneously, there are findings indicating that the tumour can initially grow by coopting existing host vessels. As the tumour grows, however, part of the initial vasculature in the internal region of the tumour regresses causing massive tumour cell death, and subsequently angiogenesis develops [4,5].

The structure of the vascular system that supplies the tumour is complex and irregular in most neoplastic tissues, so it is difficult to study the relationship between the distance from blood vessels and the cell proliferation, and therefore between the extent of vasculature and the tumour growth. In some tumours, however, it is possible to observe cylindrical arrangements of viable tumour cells, surrounded by necrosis, around blood vessels, and this simple geometry makes this study more feasible. These structures are named *tumour cords* [6-11]. In tumours that show vessel cooption, cuffs of viable tumour cells around the coopted blood vessels have been observed [4]. The mean thickness of the cords (i.e., the distance between vessel wall and necrosis) has been found to be 60–120 μm in different tumours, with a mean radius of central vessel of 10–40 μm [6-11].

The cell proliferation within the tumour cord induces migration of cells towards the periphery: cells are pushed by growing and dividing cells and eventually move into the necrotic zone. A mathematical model that describes the growth of an isolated tumour cord within a normal tissue and the formation of necrotic regions, taking into account the diffusion of a chemical critical for cell viability such as oxygen, was presented in [12]. The model predicts that a constant value for the radius of the cord will be attained in a finite time. Experimental observations have shown that the cell proliferation rate, measured by the fraction of cells in S phase and by the fraction of cells in mitosis, appears to decrease from the vessel wall to the periphery of the cord [6-8], and this phenomenon is likely to be related to the decrease of the concentration of oxygen, nutrients, and other critical chemicals. A mathematical model which describes the cell kinetics in a tumour cord at the stationary state, that is when the cord has attained the maximal radius compatible with the supply of vital substances, and the structure of the cell population is time-invariant, was proposed in [13]. In [13], the model was formulated using the age formalism and the variability of the cell cycle phase transit times was disregarded, all proliferating cells being assumed to traverse the cycle in the same time. The variability of the microenvironment within the cord was assumed to affect only the transition of cells to a quiescent postmitotic compartment.

The mathematical model for the cell population within a tumour cord at the stationary state, proposed in the present paper, takes into account the cell-to-cell variability of phase transit

times and the decrease of the rate of progression across the cell cycle that is likely to accompany the migration of cells from the region close to the central vessel to the periphery of the cord. The time courses of the labelling index and of the fraction of labelled mitoses after pulse labelling of the S–phase cells, as predicted by the model, are compared with experimental data reported in the literature.

2. The model

We will describe a tumour cord around a blood vessel of radius r_0 as a cylinder of tumour cells of radius R. At the stationary state, the radius R will represent the cord-necrosis interface. Let r denote the radial distance from the axis of the central blood vessel. As in [13], the changes of parameters and variables along the axial direction of the cord are neglected, and the tumour cord is considered as a continuous medium in which the number of tumour cells per unit volume is assumed constant in space and time. Cell motions in the axial direction are considered to be negligible, and cell migration in the radial direction is described by a velocity field $u(r,t)$, common to all cells, irrespective of cell position within the cycle and of its cycling or quiescent status.

The cell cycle of tumour cells is represented, according to the model proposed by Kendall [14] and Takahashi [15,16], by a sequence of discrete compartments of cell maturity. Let $M = \sum_i m_i$ be the total number of maturity compartments, m_i, $i = 1, \cdots, 4$, being the number of compartments in G1, S, G2, and M phases, respectively. Let λ_k, $k = 1, \cdots, M$, be the exit rate constant from compartment k. The rate constants λ_k may differ for G1, S, G2, and M phases and we will assume

$$\lambda_k = \begin{cases} \lambda_{G1} & k = 1, \cdots, m_1 \\ \lambda_S & k = m_1+1, \cdots, m_1+m_2 \\ \lambda_{G2} & k = m_1+m_2+1, \cdots, m_1+m_2+m_3 \\ \lambda_M & k = m_1+m_2+m_3+1, \cdots, M\,. \end{cases} \tag{1}$$

We assume that newborn cells can arrest their progression across the cycle and become quiescent, so that only a fraction $\theta(r,t) \in [0,1]$ of newborn cells enter the G1 phase (see Fig. 1). The dependence of θ on r and t reflects the dependence of cell arrest on the concentrations of oxygen, nutrients and other chemicals within the cord. Since in their motion towards the cord periphery cells are likely to experience more severe conditions, we will take the cell arrest as irreversible. Moreover, we assume that the rate of progression across the cycle can depend on these concentrations, so that the exit rate constants of the maturity compartments may change with r and t, although we exclude that the λ_k's can vanish. In particular, in view of the larger variability of G1 phase duration with respect to the other cycle phases [17], the cell microenvironment is likely to mainly affect the progression through that phase, so in part of the following treatment only the rate constant λ_{G1} will be considered to be varying. If a stationary state is attained, the concentration of the chemicals along the radial direction will not change with the time, and θ and the exit rate constants are functions of the radial distance only. Because of the worsening of the microenvironment when the distance from the central vessel increases, it is reasonable to assume that these functions of r are non-increasing. Although it is likely that cell death can occur within the cord when approaching the periphery, apoptosis within the cord is disregarded, assuming that at the stationary state cell death occurs immediately beyond the radius R.

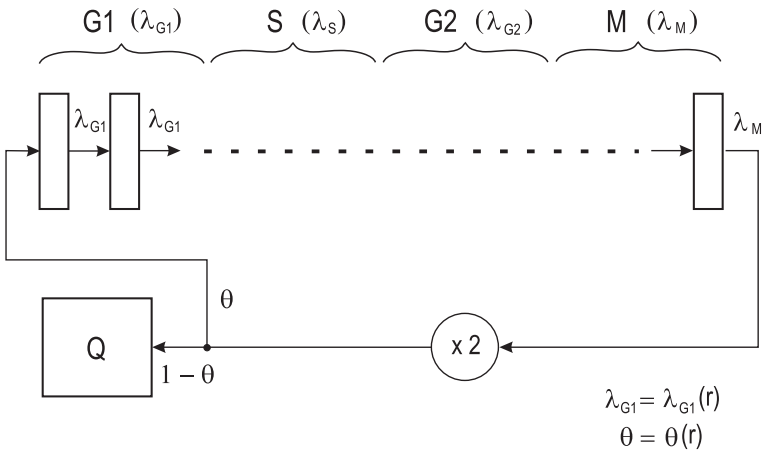

Fig. 1. Scheme of the cell population model with discrete maturity compartments and quiescent compartment. For the symbols see the text.

Denoting by $n_k(r,t)$ the number of cells in the k-th compartment, and by $n_Q(r,t)$ the number of quiescent cells, in the unit volume at distance r and time t, from the previous assumptions we can write the following conservation equations:

$$\frac{\partial n_1}{\partial t} + \frac{1}{r}\frac{\partial}{\partial r}(run_1) = 2\theta\lambda_M n_M - \lambda_1 n_1 \tag{2}$$

$$\frac{\partial n_k}{\partial t} + \frac{1}{r}\frac{\partial}{\partial r}(run_k) = \lambda_{k-1} n_{k-1} - \lambda_k n_k\,, \quad k = 2, \cdots, M \tag{3}$$

$$\frac{\partial n_Q}{\partial t} + \frac{1}{r}\frac{\partial}{\partial r}(run_Q) = 2(1-\theta)\lambda_M n_M\,. \tag{4}$$

Moreover, denoting by $n(r,t)$ the total cell density at r and t, we have

$$\frac{\partial n}{\partial t} + \frac{1}{r}\frac{\partial}{\partial r}(run) = \lambda_M n_M\,. \tag{5}$$

By assuming that n is constant and equal to $\bar{n}$, and that $u(r_0,t) = 0$ (i.e., there is no cell flux across the vessel wall), $u(r,t)$ can be derived from Eq. (5) as

$$ru(r,t) = \frac{1}{\bar{n}}\int_{r_0}^{r} z\lambda_M(z,t)n_M(z,t)\,dz\,. \tag{6}$$

In contrast with the present model, we will denote as "Takahashi model" the cell population model with cell cycle structure as in Fig. 1, but without spatial structure and cell migration. In a stochastic framework, according to this model cells spend in the maturity compartments random times that are independent and exponentially distributed with parameter λ_k. Thus, under the assumption (1), the time spent in each cell cycle phase has a gamma distribution with, e.g. for G1 phase, mean value equal to m_1/λ_{G1} and coefficient of variation $m_1^{-1/2}$. The expected values of the number of cells in the maturity compartments of cell cycle and in the quiescent state are given in the Takahashi model by the solution of a set of ODE's whose right hand side is the same as that of Eqs. (2)-(4). We note that, in deriving the distribution of times spent by cells in the cell cycle phases within a tumour cord, it should be taken into account that the maximal life span of a cell is equal to the time needed to migrate from the position at birth

to the boundary with the necrotic zone (and thus is finite if the cell is born at $r > r_0$) and that the rate of exit from a maturity compartment can be varying with the time.

3. Stationary state

Experimental data suggest that in most of the observed tumour cords the cord radius is constant with the time. We will assume that in these cords also the maturity distribution is in a stationary state, i.e. it is time-invariant, so that $n_k(r,t) = n_k(r)$. Let $f_k(r) = n_k(r)/\bar{n}$ be the fraction of cells in the k-th compartment of maturity at distance r in the stationary state. The conservation equations become

$$\frac{1}{r}\frac{d}{dr}(ruf_1) = 2\theta\lambda_M f_M - \lambda_1 f_1 \tag{7}$$

$$\frac{1}{r}\frac{d}{dr}(ruf_k) = \lambda_{k-1} f_{k-1} - \lambda_k f_k\,, \quad k = 2, \cdots, M \tag{8}$$

$$\frac{1}{r}\frac{d}{dr}(ruf_Q) = 2(1-\theta)\lambda_M f_M \tag{9}$$

with

$$ru(r) = \int_{r_0}^{r} z\lambda_M f_M\, dz\,. \tag{10}$$

The above equations can be rewritten in the following form:

$$\left(\frac{1}{r}\int_{r_0}^{r} z\lambda_M f_M\, dz\right)\frac{df_1}{dr} = 2\theta\lambda_M f_M - \lambda_1 f_1 - \lambda_M f_M f_1 \tag{11}$$

$$\left(\frac{1}{r}\int_{r_0}^{r} z\lambda_M f_M\, dz\right)\frac{df_k}{dr} = \lambda_{k-1} f_{k-1} - \lambda_k f_k - \lambda_M f_M f_k\,, \quad k = 2, \cdots, M \tag{12}$$

$$\left(\frac{1}{r}\int_{r_0}^{r} z\lambda_M f_M\, dz\right)\frac{df_Q}{dr} = 2(1-\theta)\lambda_M f_M - \lambda_M f_M f_Q\,. \tag{13}$$

Equations (7)-(10) are a nonlinear system of integro-differential type with degeneracy at $r = r_0$, since $u(r)$ vanishes there. However, in the case in which θ and all the rate constants λ_k are constant, it is easy to see that there exists a unique solution which is constant with r. Let $\bar{f}_k$, $k = 1, \cdots, M$, be this constant solution. From (11)-(12), we obtain the following equations:

$$2\theta\lambda_M \bar{f}_M - \lambda_1 \bar{f}_1 - \lambda_M \bar{f}_M \bar{f}_1 = 0 \tag{14}$$

$$\lambda_{k-1}\bar{f}_{k-1} - \lambda_k \bar{f}_k - \lambda_M \bar{f}_M \bar{f}_k = 0\,, \quad k = 2, \cdots, M\,, \tag{15}$$

from which we have

$$\bar{f}_1 = \frac{2\theta\lambda_M}{\lambda_1 + \lambda_M \bar{f}_M}\bar{f}_M \tag{16}$$

$$\bar{f}_k = \frac{\lambda_{k-1}}{\lambda_k + \lambda_M \bar{f}_M}\bar{f}_{k-1}\,, \quad k = 2, \cdots, M\,. \tag{17}$$

Supposing $\bar{f}_M$ assigned, Eqs. (14)-(15) are linear in $\bar{f}_k$, $k = 1, \cdots, M$ so that a nonzero solution will exist if and only if the determinant of coefficients is zero. By computing this determinant, we obtain that $\bar{f}_M$ must satisfy the equation

$$\prod_{k=1}^{M} \frac{\lambda_k + \lambda_M \bar{f}_M}{\lambda_k} = 2\theta\,. \tag{18}$$

If $0.5 < \theta \leq 1$, the above equation has a real positive solution that is unique and less than one. Thus, from Eqs. (16)-(17), all the fractions $\bar{f}_k$ can be determined. By summing (14)-(15), we have $\sum_{m=1}^{M} \bar{f}_k = 2\theta - 1 \leq 1$. From (13), we obtain $\bar{f}_Q = 2(1-\theta)$ and thus $\sum_{m=1}^{M} \bar{f}_k + \bar{f}_Q = 1$. We note that the fractions $\bar{f}_k$ are the same as the fractions obtained from the solution in asynchronous exponential growth of the Takahashi model with the same parameter values.

In the general case of θ and λ_k dependent on r, because of the degeneracy at r_0, it is not possible to prescribe data for $r = r_0$, and the values of the unknown functions $f_k(r)$ at $r = r_0$ (denoted by f_k^0, $k = 1, \cdots, M$) must be deduced from suitable conditions. We will impose that the right derivative of the solution at r_0 is bounded. Thus the values of f_k^0 turn out to be precisely the ones given by Eqs. (16)-(18) with θ and λ_k evaluated at r_0. We will take $\theta(r_0) > 0.5$, which is necessary and sufficient to have f_k^0 positive. If we assume that $\theta(r)$ and the coefficients $\lambda_k(r)$ have enough regularity, knowing their derivatives up to some order at $r = r_0$, it is possible to calculate the derivatives at r_0 of the possible solutions of (7), (8) and (10) up to the same order. We show the procedure for the first derivative in Appendix A.

Assuming the existence of the solution, we now establish the qualitative results:

$$0 < f_k(r) < 1\,, \quad k = 1, \cdots, M\,, \quad 0 \leq f_Q(r) < 1\,, \tag{19}$$

$$\sum_{k=1}^{M} f_k(r) + f_Q(r) = 1\,. \tag{20}$$

First we show that $f_k > 0$. This is true for $r = r_0$. Suppose that f_j is the first function in the set $(f_1 \cdots f_M)$ that vanishes at the point $r_j > r_0$. For $j > 1$, using (12) we obtain $df_j/dr|_{r=r_j} > 0$, unless $f_{j-1}(r_j) = 0$, and for $j = 1$ we need $f_M(r_j) = 0$ to avoid a positive derivative. In other words, all the functions must vanish simultaneously. Integrating (11)-(12) backward from r_j, we can see, however, that this fact is compatible only with $f_k \equiv 0$ for every k, contradicting the initial values. Concerning f_Q, it is $f_Q \geq 0$ at r_0. For $r > r_0$, from (13) it is $df_Q/dr > 0$ if $f_Q(r) < 0$. Thus f_Q cannot become negative. We now prove $f_k < 1$ and $f_Q < 1$ showing that $F = \sum_{k=1}^{M} f_k + f_Q = 1$. This is true for $r = r_0$. From Eqs. (11)-(13), the equation satisfied by F is

$$u \frac{dF}{dr} = (1 - F)\lambda_M f_M\,. \tag{21}$$

This equation shows that F is increasing in the set $\{r : F < 1\}$ and decreasing in the set $\{r : F > 1\}$. Now, if one of these sets is not empty we see, integrating backward, that the condition $F(r_0) = 1$ cannot be matched. Then F must be constant and equal to 1. The existence and uniqueness of the solution of Eqs. (7)-(10) is under study.

To obtain a numerical solution of Eqs. (7), (8) and (10), we note that these equations can be rewritten as the following set of integral equations:

$$\left(\int_{r_0}^{r} z\lambda_M f_M\, dz\right) f_1(r) = 2\int_{r_0}^{r} z\theta\lambda_M f_M\, dz - \int_{r_0}^{r} z\lambda_1 f_1\, dz \tag{22}$$

$$\left(\int_{r_0}^{r} z\lambda_M f_M\, dz\right) f_k(r) = \int_{r_0}^{r} z\lambda_{k-1} f_{k-1}\, dz - \int_{r_0}^{r} z\lambda_k f_k\, dz\,, \quad k = 2, \cdots, M\,. \tag{23}$$

A solution of the above equations can be obtained by an iterative procedure. We define as x the vector of all the values $f_k(r_i)$, $k = 1, \cdots, M$, r_i being equispaced mesh points in $[r_0, R]$, and

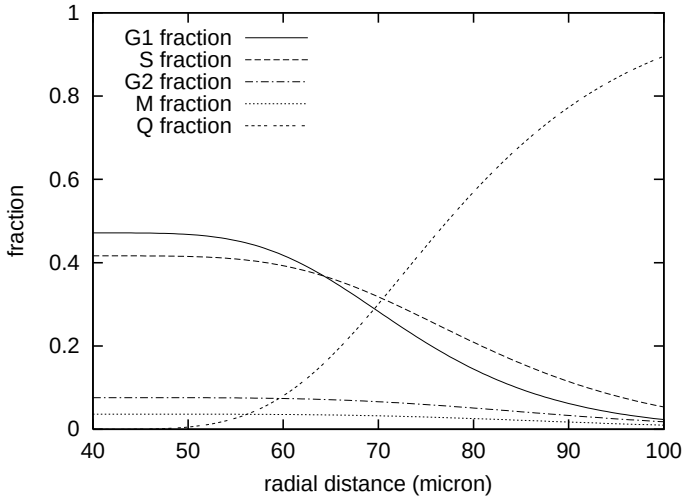

Fig. 2. Cell cycle phase fractions and fraction of quiescent cells in the stationary state as a function of radial distance. Kinetic parameters: $m_1 = 2$, $m_2 = 9$, $m_3 = m_4 = 2$, $\lambda_{G1} = 0.25\,\mathrm{h}^{-1}$, $\lambda_S = 1.0\,\mathrm{h}^{-1}$, $\lambda_{G2} = 1.0\,\mathrm{h}^{-1}$, $\lambda_M = 2.0\,\mathrm{h}^{-1}$, and $\theta(r) = 1/(1 + 16((r - r_0)/(R - r_0))^4)$. Geometric parameters: $r_0 = 40\,\mu$m, $R = 100\,\mu$m.

rewrite Eqs. (22)-(23) as $x = G(x)$, computing the integrals by the trapezoidal rule. This system of algebraic equations was solved using the iteration [18]

$$x^{n+1} = x^n + \alpha(G(x^n) - x^n)\,, \tag{24}$$

where x^n denotes the solution at the n-th step. The convergence (that resulted very slow indeed) was achieved with small positive α.

Figure 2 represents the steady-state fractions of cells in the G1, S, G2, and M phases, obtained by summing the fractions $f_k(r)$ over the appropriate indexes, and the quiescent fraction $f_Q(r)$. The kinetic and geometric parameters of the simulated tumour cord are reported in the figure legend. It can be observed that the ratios of the phase fractions with respect to the fraction of proliferating cells are not constant with r.

An experimental technique largely used to study the cell proliferation within tumour cords is based on the measurement of the fraction of cells in S phase at various radial distances, obtained as the fraction of labelled cells immediately after the injection of a radioactive DNA precursor, or of the fraction in M phase, obtained by examination of histological slices of the tumour [6-8]. Thus, the question arises if these data allow to distinguish whether there is a decelerated progression through G1 phase, as the radial distance increases, or there is an increase in the fraction of postmitotically arrested cells, when all the other cell cycle parameters are constant with r. We prove that this is not possible, see Appendix B, as far as the S and M phase fractions at the stationary state are considered. However, the technique of labelling S-phase cells followed by autoradiography also allows to measure the time course of the fraction of labelled cells as well as the fraction of labelled cells in mitosis. As we will see in the following, the time evolution of these fractions can be different if a decreasing rate of progression in G1 or a true postmitotic cell arrest occurs.

4. Pulse labelling

The injection of a labelled DNA precursor will label tumour cells in a way that can be considered equivalent in practice to a true impulsive labelling. If the injection occurs at $t=0$, we will assume that at $t=0^+$ all (and only) S-phase cells are labelled. Thereafter, the subpopulation of labelled cells progresses through the cycle and cells undergo division: we will assume that, at each division, cells generated by labelled cells remain labelled.

Let $f_k^l(r,t)$ be the fraction of labelled cells in the k-th compartment at distance r and time t. We will assume here that the exit rate constants λ_S, λ_{G2} and λ_M are constant with r. By writing the conservation equations for the labelled subpopulation in all the maturity compartments and in the quiescent compartment, we obtain for the time evolution of the labelled fractions the following equations:

$$\frac{\partial f_1^l}{\partial t} + \frac{1}{r}\frac{\partial}{\partial r}(ruf_1^l) = 2\theta\lambda_M f_M^l - \lambda_1 f_1^l \tag{25}$$

$$\frac{\partial f_k^l}{\partial t} + \frac{1}{r}\frac{\partial}{\partial r}(ruf_k^l) = \lambda_{k-1} f_{k-1}^l - \lambda_k f_k^l\,, \quad k=2,\cdots,M \tag{26}$$

$$\frac{\partial f_Q^l}{\partial t} + \frac{1}{r}\frac{\partial}{\partial r}(ruf_Q^l) = 2(1-\theta)\lambda_M f_M^l \tag{27}$$

where

$$ru(r) = \lambda_M \int_{r_0}^{r} z f_M(z)\,dz\,, \tag{28}$$

with the initial conditions

$$f_k^l(r,0) = \begin{cases} f_k(r) & k = m_1+1,\cdots,m_1+m_2 \\ 0 & \text{otherwise,} \end{cases} \qquad f_Q^l(r,0) = 0\,. \tag{29}$$

Since we assume that cell labelling occurs in a population at the stationary state, the functions $f_k(r)$ and $u(r)$ in the above equations are the fractions of cells and the velocity field in the stationary state, as defined in the previous section.

Equations (25)-(27) can be rewritten as

$$\frac{\partial f_1^l}{\partial t} + u\frac{\partial f_1^l}{\partial r} = 2\theta\lambda_M f_M^l - \lambda_1 f_1^l - \lambda_M f_M f_1^l \tag{30}$$

$$\frac{\partial f_k^l}{\partial t} + u\frac{\partial f_k^l}{\partial r} = \lambda_{k-1} f_{k-1}^l - \lambda_k f_k^l - \lambda_M f_M f_k^l\,, \quad k=2,\cdots,M \tag{31}$$

$$\frac{\partial f_Q^l}{\partial t} + u\frac{\partial f_Q^l}{\partial r} = 2(1-\theta)\lambda_M f_M^l - \lambda_M f_M f_Q^l\,. \tag{32}$$

Equations (30)-(32) are a system of first-order and linear equations, whose characteristic lines tend to have vanishing slope as $r \to r_0$. Thus the initial conditions (29) determine completely the solution for $t \geq 0$ and $r \in (r_0, R]$. For $r = r_0$, by denoting $f_k^{l0}(t) = f_k^l(r_0,t)$ and $f_Q^{l0}(t) = f_Q^l(r_0,t)$, we have

$$\frac{df_1^{l0}}{dt} = 2\theta(r_0)\lambda_M f_M^{l0} - \lambda_{G1}(r_0) f_1^{l0} - \lambda_M f_M^0 f_1^{l0} \tag{33}$$

$$\frac{df_k^{l0}}{dt} = \lambda_{G1}(r_0) f_{k-1}^{l0} - \lambda_{G1}(r_0) f_k^{l0} - \lambda_M f_M^0 f_k^{l0}\,, \quad k=2,\cdots,m_1 \tag{34}$$

$$\frac{df^{l0}_{m_1+1}}{dt} = \lambda_{G1}(r_0) f^{l0}_{m_1} - \lambda_{m_1+1} f^{l0}_{m_1+1} - \lambda_M f^0_M f^{l0}_{m_1+1} \tag{35}$$

$$\frac{df^{l0}_k}{dt} = \lambda_{k-1} f^{l0}_{k-1} - \lambda_k f^{l0}_k - \lambda_M f^0_M f^{l0}_k\,, \quad k = m_1+2, \cdots, M \tag{36}$$

$$\frac{df^{l0}_Q}{dt} = 2(1-\theta(r_0))\lambda_M f^{l0}_M - \lambda_M f^0_M f^{l0}_Q\,, \tag{37}$$

with the initial conditions

$$f^{l0}_k(0) = \begin{cases} f^0_k & k = m_1+1, \cdots, m_1+m_2 \\ 0 & \text{otherwise,} \end{cases} \qquad f^{l0}_Q(0) = 0\,. \tag{38}$$

The numerical solution of Eqs. (25)-(29) was computed by a finite–difference scheme over a rectangular grid with fixed mesh size on $[0,T]\times[r_0,R]$. Time derivatives were approximated by forward differences whereas spatial derivatives by backward differences. The scheme required the knowledge of the solution at $r=r_0$, and this is given by the solution of equations (33)-(38).

The time evolution of the fractions of labelled cells allows to compute the evolution at different radial distances of various observable quantities, such as the total fraction of labelled cells, $LI(r,t)$, and the fraction of labelled cells within the cells in mitosis, $FLM(r,t)$, according to

$$LI(r,t) = \sum_{k=1}^{M} f^l_k(r,t) + f^l_Q(r,t)\,, \qquad FLM(r,t) = \frac{\displaystyle\sum_{k=M-m_4+1}^{M} f^l_k(r,t)}{\displaystyle\sum_{k=M-m_4+1}^{M} f_k(r)}\,. \tag{39}$$

Numerical simulations have shown that, for large t, LI and FLM converge to a common value which is independent of r. Because Eqs. (25)-(28) admit stationary solutions of the form $f^l_k(r) = cf_k(r)$ and $f^l_Q(r) = cf_Q(r)$ with $0 \le c \le 1$, the observed behaviour suggests that the solution of (25)-(29) tends to a stationary solution with c depending on the initial condition. If it is so, it is easy to see from Eq. (39) that both $LI(r,t)$ and $FLM(r,t)$ will tend to c independently of r.

5. Application to experimental data

We applied the above model to the analysis of experimental data reported by Hirst and Denekamp in [7]. These data have been obtained from the KHH mammary carcinoma, a tumour that grows in mice showing a corded structure. As reported in [7], when the tumour reached a diameter of 7.5–10 mm, the animals were injected with ^{3}H-thymidine and, at different times after label injection, the animals were sacrificed and the tumours excised. Histological sections were scanned and cells categorized in relation to the nearest visible blood vessel. Three classes were distinguished: cells close to vessels, cells close to necrosis and cells in the intermediate zones. The fraction of labelled cells (labelling index, LI) and the fraction of labelled mitoses (FLM) were measured in the three above defined zones up to 50 hours after label injection.

The LI and FLM data were analyzed under two different hypotheses. First, we assumed that progression across the G1 phase of cell cycle is not affected by the radial distance of cells, whereas θ decreases with r. Alternatively, we assumed that λ_{G1} is affected by the radial distance whereas no cell arrest occurs (i.e., $\theta(r)=1$).

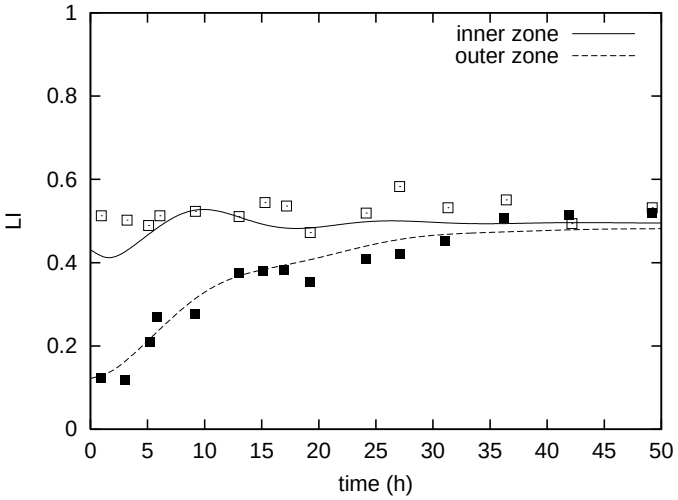

Fig. 3. Experimental data of LI as a function of time in the inner (open squares) and the outer zone (black squares) of the cord. Data replotted from Hirst and Denekamp [7]. Model predictions with λ_{G1} constant and θ dependent on r (continuous lines). The function $\theta(r)$ and the parameter values are reported in the text.

Under the first hypothesis, using a trial-and-error procedure, a reasonable fitting of the data was obtained with the following choice of parameter values: $m_1 = 2$, $m_2 = 9$, $m_3 = m_4 = 2$, $\lambda_{G1} = 0.278\,\mathrm{h}^{-1}$, $\lambda_S = 1.059\,\mathrm{h}^{-1}$, $\lambda_{G2} = 1.333\,\mathrm{h}^{-1}$, $\lambda_M = 3.333\,\mathrm{h}^{-1}$, and $\theta(r)$ given by

$$\theta(r) = \frac{1}{1 + 16((r - r_0)/(R - r_0))^4}\,. \tag{40}$$

The geometric parameters of the cord were $r_0 = 40\,\mu$m and $R = 100\,\mu$m, according to the average measured diameters. The values chosen for the m_i's and the exit rate constants are such that the mean values of T_{G1}, T_S, T_{G2} and T_M are 7.2 h, 8.5 h, 1.5 h and 0.6 h, respectively, that is the phase transit times estimated in [7] for the cells in the inner zone of the cord. Figure 3 shows the behaviour of LI in the inner and the outer zone of the cord. The predicted time course was calculated at $r = 50\,\mu$m and at $r = 90\,\mu$m, respectively. In Fig. 4, the experimental FLM data are shown together with their predictions. We note, in particular, that the theoretical prediction of the FLM curve in the outer zone fails to follow the rising front of the second wave of experimental data.

Under the second hypothesis, data were fitted by choosing the following values of the parameters: $m_1 = 2$, $m_2 = 7$, $m_3 = m_4 = 2$, λ_S, λ_{G2} and λ_M as before, $\lambda_{G1}(r)$ given by

$$\lambda_{G1}(r) = -0.1 + \frac{0.55}{1 + 4.5((r - r_0)/(R - r_0))^{1.5}}\ \ \mathrm{h}^{-1}\,, \tag{41}$$

and $\theta(r) = 1$. The time course of the prediction of the labelling index data is depicted in Fig. 5, showing a fitting of comparable quality with respect to the fitting obtained with θ dependent on r. In the prediction of the FLM curve in the outer zone of the cord, the rising front of the second wave appears now to be delayed as shown by the data (see Fig. 6).

It can be surprising that the second wave of the predicted FLM curve in the outer zone (Fig. 6) is so slightly delayed, considering that the value of λ_{G1} at $90\,\mu$m, as given by Eq. (41),

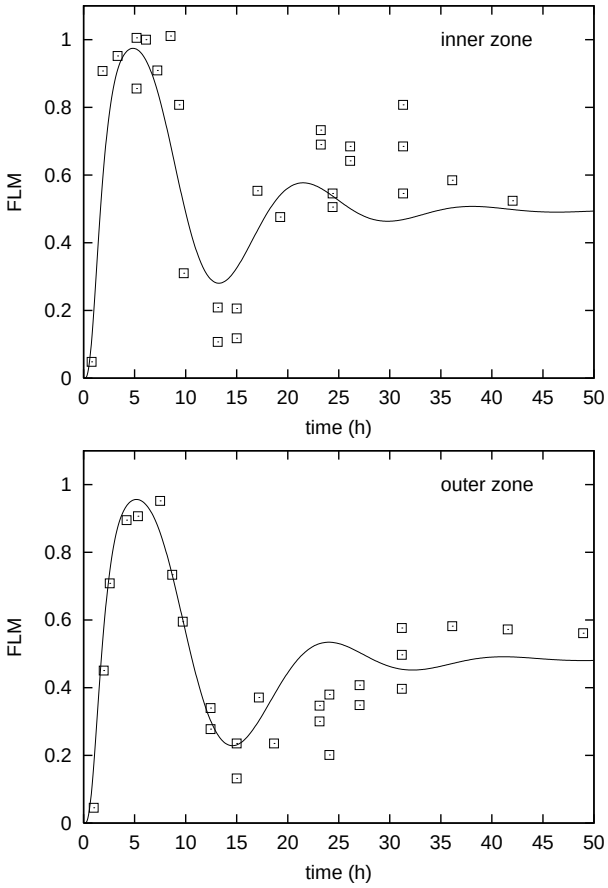

Fig. 4. Experimental data of FLM (squares) as a function of time in the inner (upper panel) and the outer zone (lower panel) of the cord. Data replotted from Hirst and Denekamp [7]. Model predictions with λ_{G1} constant and θ dependent on r (continuous lines). The function $\theta(r)$ and the parameter values are reported in the text.

is 0.0243 h^{-1}, which would correspond in the Takahashi model to a mean T_{G1} of 82.3 h (whereas λ_{G1} at 50 μm is 0.321 h^{-1}, corresponding to a mean T_{G1} of 6.2 h). This behaviour is due to the cell migration within the cord. To show the effect of cell migration on the time course of FLM, we compared the response of our model at $r = 50\,\mu$m and $r = 90\,\mu$m to the FLM curves predicted by the Takahashi model (i.e., a model without cell migration) having λ_{G1} equal to $\lambda_{G1}(r)$ at $r = 50\,\mu$m and $r = 90\,\mu$m, respectively, and the other parameters unchanged. Figure 7 shows this comparison: whereas the FLM curve in the inner zone slightly differs from that predicted by the Takahashi model, the difference is very marked when the FLM curve in the outer zone of the cord is considered, where the FLM predicted by the present model shows a moderate delay of the second wave. This marked difference can be explained considering that the labelled mitoses observed in the outer zone of the cord are the mitoses of cells that have spent the $G1$ phase at smaller radial distances where the progression across G1 phase is faster. In other words, because of cell migration, the mean cell cycle duration of cells dividing at the periphery will be shorter than that of non-moving cells characterized by the cell kinetic parameters of the cord periphery.

Without taking into account cell migration, previous analyses of the FLM curves, based on

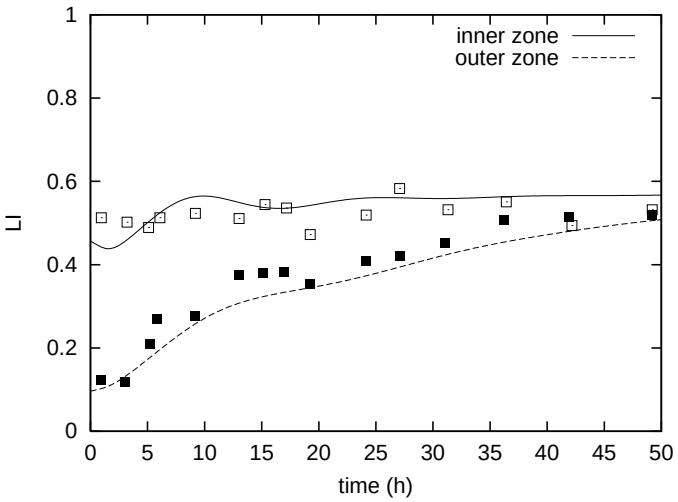

Fig. 5. Experimental data of LI as in Fig. 3. Model predictions with $\theta = 1$ and λ_{G1} dependent on r (continuous lines). The function $\lambda_{G1}(r)$ and the parameter values are reported in the text.

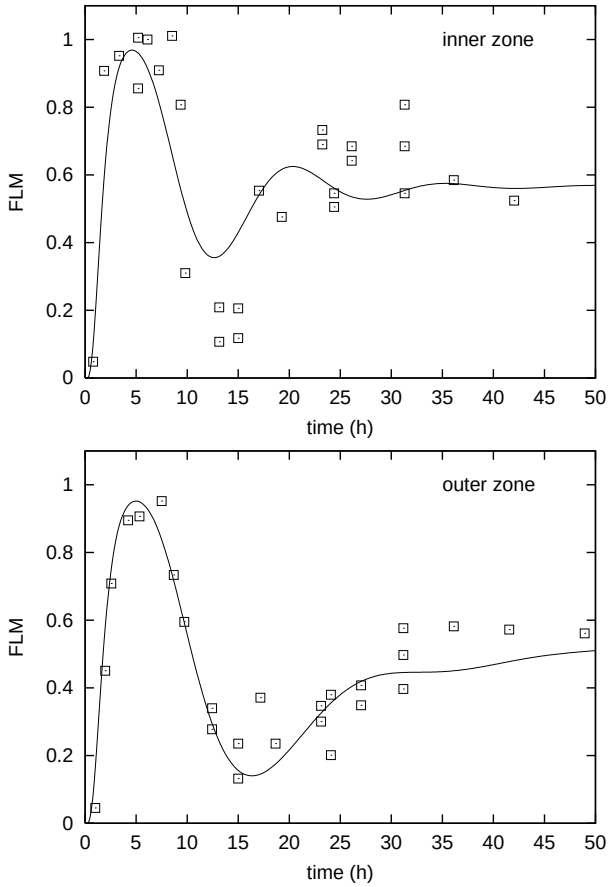

Fig. 6. Experimental data of FLM (squares) as in Fig. 4. Model predictions with $\theta = 1$ and λ_{G1} dependent on r (continuous lines). The function $\lambda_{G1}(r)$ and the parameter values are reported in the text.

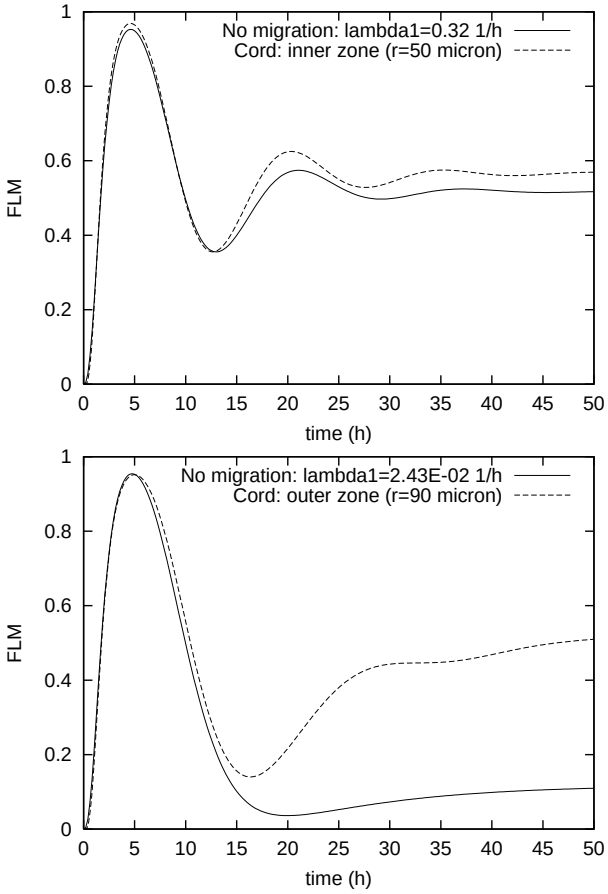

Fig. 7. Comparison between the FLM curves predicted by the model of the tumour cord (dashed lines) and the FLM curves predicted by the Takahashi model (continuous lines): inner zone (upper panel), outer zone (lower panel). For the values of the parameters see the text.

cell population models similar to the Takahashi model, had found no difference [6] or only slight differences [7] in the kinetic parameters of cell cycle in regions proximal to the central vessel and in regions at the periphery of the cord.

6. Concluding remarks

The analysis of labelling data here proposed suggests that, because of the decay of oxygen and nutrient concentration in tumour cords, the progression across cell cycle is slowed down as the distance from the central vessel increases. We have found that the retarded progression suggested by the experimental data can be achieved in the model by suitably lowering only the rate of progression in G1.

In the presence of decreased rates of progression through cell cycle phases at the periphery of tumour cords, the kinetic differences between inner and outer zones can be largely masked by cell migration when data from pulse labelling are considered. Thus, more in general, our results indicate that a correct analysis of data from tumour microregions requires that the possible cell migration through these regions has to be taken into account.

Finally, we note that the continuous-medium approach here adopted was able to describe substantially the experimental data considered, although the size of the particles (the cells) is comparable in the tumour cords to the spatial scale. An approach based on the behaviour of individual cells could, however, improve the description of cell motion, in particular near the wall of the central vessel.

Acknowledgements: The support of the Progetto Strategico del CNR "Metodi e Modelli Matematici per lo Studio dei Fenomeni Biologici" is gratefully acknowledged.

Appendix A

We show here how to compute the first right derivative at $r = r_0$, denoted as $f_k'^0$, of the solution f_k of Eqs. (7), (8) and (10), assuming that the functions $\theta(r)$ and $\lambda_k(r)$ have enough regularity. Let us insert in (7), (8) and (10) the first order approximations

$$\theta(r) \simeq \theta^0 + \theta'^0(r - r_0)\,, \quad \lambda_k(r) \simeq \lambda_k^0 + \lambda_k'^0(r - r_0)\,, \quad k = 1, \cdots, M$$

where $\theta^0 = \theta(r_0)$, $\theta'^0 = \theta'(r_0)$, and $\lambda_k^0 = \lambda_k(r_0)$, $\lambda_k'^0 = \lambda_k'(r_0)$, and look for the first-order approximation

$$f_k(r) \simeq f_k^0 + f_k'^0(r - r_0)\,, \quad k = 1, \cdots, M\,. \tag{A.1}$$

From $\operatorname{div} u = \lambda_M f_M$, we deduce

$$\operatorname{div} u \simeq \lambda_M^0 f_M^0 + (\lambda_M^0 f_M'^0 + \lambda_M'^0 f_M^0)(r - r_0) \tag{A.2}$$

and, from Eq. (10),

$$u \simeq \frac{1}{r}\lambda_M^0 f_M^0 \frac{r^2 - r_0^2}{2} \simeq \lambda_M^0 f_M^0 (r - r_0)\,. \tag{A.3}$$

Using all the above approximations in (7)-(8), the zero order terms cancel because of (14)-(15) written with θ and λ_k evaluated at r_0. Equating the first order terms we arrive at the system

$$f_1'^0(2\lambda_M^0 f_M^0 + \lambda_1^0) = -f_1^0(\lambda_M'^0 f_M^0 + \lambda_1'^0) + 2f_M^0(\theta'^0\lambda_M^0 + \theta^0\lambda_M'^0) + f_M'^0(2\theta^0\lambda_M^0 - f_1^0\lambda_M^0) \tag{A.4}$$

$$f_k'^0(2\lambda_M^0 f_M^0 + \lambda_k^0) = -f_k^0(\lambda_M'^0 f_M^0 + \lambda_k'^0) + \lambda_{k-1}'^0 f_{k-1}^0 - f_M'^0 f_k^0 \lambda_M^0 - \lambda_{k-1}^0 f_{k-1}'^0\,, \quad k = 2, \cdots, M \tag{A.5}$$

which defines $f_k'^0$, $k = 2, \cdots, M-1$, recursively in terms of $f_1'^0$ and $f_M'^0$ by means of

$$\lambda_k^0 f_k'^0 = -\sum_{i=0}^{k-1}\Big(\prod_{j=k-i}^{k}\frac{\lambda_j^0}{a_j}\Big)b_{k-i}f_{k-i}^0 - \lambda_M^0 f_M'^0\sum_{i=0}^{k-1}\Big(\prod_{j=k-i}^{k}\frac{\lambda_j^0}{a_j}\Big)b_{k-i}f_{k-i}^0$$

$$+\sum_{i=0}^{k-2}\prod_{j=k-i}^{k}\lambda_{k-i-1}'^0 f_{k-i-1}^0 + \lambda_1^0\Big(\prod_{j=2}^{k}\frac{\lambda_j^0}{a_j}\Big)f_1'^0\,, \quad k = 2, \cdots, M\,, \tag{A.6}$$

where $a_j = 2\lambda_M^0 f_M^0 + \lambda_j^0$ and $b_k = \lambda_M'^0 f_M^0 + \lambda_k'^0$. Using (A.6) for $k = M$ and replacing $f_1'^0$ by the expression deduced from $(A.4)$, we obtain the equality:

$$\lambda_M^0 f_M'^0\Big[1 + \sum_{i=0}^{M-1}\Big(\prod_{j=M-i}^{M}\frac{\lambda_j^0}{a_j}\Big)f_{M-i}^0\Big] = -\sum_{i=0}^{M-1}\Big(\prod_{j=M-i}^{M}\frac{\lambda_j^0}{a_j}\Big)b_{M-i}f_{M-i}^0$$

$$+\sum_{i=0}^{M-2}\prod_{j=M-i}^{M}\lambda'^0_{M-i-1}f^0_{M-i-1}+\left(\prod_{j=1}^{M}\frac{\lambda^0_j}{a_j}\right)\left[-f^0_1(\lambda'^0_M f^0_M+\lambda'^0_1)\right.$$
$$\left.+2f^0_M(\theta'^0\lambda^0_M+\theta^0\lambda'^0_M)+\lambda^0_M f'^0_M(2\theta^0-f^0_1)\right]. \qquad (A.7)$$

At this point we note that

$$\left(\prod_{j=1}^{M}\frac{\lambda^0_j}{a_j}\right)(2\theta^0-f^0_1)<1-\frac{f^0_1}{2\theta^0}<1\,,$$

owing to (18) and taking into account that $a_j>\lambda^0_M f^0_M+\lambda^0_j$, and that

$$1-\frac{f^0_1}{2\theta^0}=\frac{\lambda^0_1}{\lambda^0_1+\lambda^0_M f^0_M}<1$$

because of (16). Thus, by rearranging $(A.7)$, it can be seen that the coefficient of f'^0_M is positive. Therefore $(A.7)$ can be solved for f'^0_M and all the other unknowns f'^0_k can be calculated. We remark that, if $\theta'^0=\lambda'^0_k=0$, $k=1,\cdots,M$, then $f'^0_k=0$ for all k. Following the above procedure higher order derivatives can be calculated, of course their expressions will be much more complicated.

Appendix B

The following proposition shows that, at the stationary state, the same behaviour of the fractions in S, G2 and M phases with the radial distance can be given by different pairs of the functions $\theta(r)$ and $\lambda_{G1}(r)$, when λ_S, λ_{G2} and λ_M are constant with r.

Proposition 1. *Given $\lambda_{G1}(r)$, $\theta(r)$, and λ_S, λ_{G2} and λ_M constant, let $f_k(r)$, $k=1,\cdots,M$, be the solution of Eqs. (7), (8) and (10). A function $\tilde\lambda_{G1}(r)$ can be found such that Eqs. (7), (8) and (10), with*

$$\tilde\theta(r)=1,\quad \tilde\lambda_S=\lambda_S,\quad \tilde\lambda_{G2}=\lambda_{G2},\quad \tilde\lambda_M=\lambda_M\,, \qquad (B.1)$$

have the solution $\tilde f_k(r)$, $k=1,\cdots,M$, with the following property

$$\tilde f_k(r)=f_k(r)\,,\quad k=m_1+1,\cdots,M\,. \qquad (B.2)$$

Proof. In view of $(B.1)$, the fractions $\tilde f_k(r)$ will satisfy the equations

$$\frac{1}{r}\frac{d}{dr}(r\tilde u\tilde f_1)=2\lambda_M\tilde f_M-\tilde\lambda_{G1}\tilde f_1 \qquad (B.3)$$
$$\frac{1}{r}\frac{d}{dr}(r\tilde u\tilde f_k)=\tilde\lambda_{G1}\tilde f_{k-1}-\tilde\lambda_{G1}\tilde f_k\,,\quad k=2,\cdots,m_1 \qquad (B.4)$$
$$\frac{1}{r}\frac{d}{dr}(r\tilde u\tilde f_{m_1+1})=\tilde\lambda_{G1}\tilde f_{m_1}-\lambda_{m_1+1}\tilde f_{m_1+1} \qquad (B.5)$$
$$\frac{1}{r}\frac{d}{dr}(r\tilde u\tilde f_k)=\lambda_{k-1}\tilde f_{k-1}-\lambda_k\tilde f_k\,,\quad k=m_1+2,\cdots,M \qquad (B.6)$$

with

$$r\tilde u(r)=\lambda_M\int_{r_0}^{r}z\tilde f_M\,dz\,. \qquad (B.7)$$

For $r=r_0$, the values $\tilde{f}_k^0$ of the solution $\tilde{f}_k$ of Eqs. $(B.3)$-$(B.7)$ will be given by

$$\tilde{f}_1^0 = \frac{2\lambda_M}{\tilde{\lambda}_{G1}^0 + \lambda_M \tilde{f}_M^0} \tilde{f}_M^0 \tag{B.8}$$

$$\tilde{f}_k^0 = \frac{\tilde{\lambda}_{G1}^0}{\tilde{\lambda}_{G1}^0 + \lambda_M \tilde{f}_M^0} \tilde{f}_{k-1}^0 \,, \quad k = 2, \cdots, m_1 \tag{B.9}$$

$$\tilde{f}_{m_1+1}^0 = \frac{\tilde{\lambda}_{G1}^0}{\lambda_{m_1+1} + \lambda_M \tilde{f}_M^0} \tilde{f}_{m_1}^0 \tag{B.10}$$

$$\tilde{f}_k^0 = \frac{\lambda_{k-1}}{\lambda_k + \lambda_M \tilde{f}_M^0} \tilde{f}_{k-1}^0 \,, \quad k = m_1+2, \cdots, M \,, \tag{B.11}$$

where $\tilde{\lambda}_{G1}^0 = \tilde{\lambda}_{G1}(r_0)$. We will search the value $\tilde{\lambda}_{G1}^0$ that yields $\tilde{f}_M^0 = f_M^0$. Expressing $\tilde{f}_M^0$ by means of $(B.8)$-$(B.11)$, we obtain the equation

$$\left(\prod_{k=m_1+1}^{M} \frac{\lambda_k + \lambda_M \tilde{f}_M^0}{\lambda_k} \right) \left(\frac{\tilde{\lambda}_{G1}^0 + \lambda_M \tilde{f}_M^0}{\tilde{\lambda}_{G1}^0} \right)^{m_1} = 2 \,, \tag{B.12}$$

and similarly, for f_M^0, we have the equation

$$\left(\prod_{k=m_1+1}^{M} \frac{\lambda_k + \lambda_M f_M^0}{\lambda_k} \right) \left(\frac{\lambda_{G1}^0 + \lambda_M f_M^0}{\lambda_{G1}^0} \right)^{m_1} = 2\theta^0 \,, \tag{B.13}$$

where $\lambda_{G1}^0 = \lambda_{G1}(r_0)$ and $\theta^0 = \theta(r_0)$. From Eqs. $(B.12)$-$(B.13)$, by setting $\tilde{f}_M^0 = f_M^0$, we obtain

$$\frac{\tilde{\lambda}_{G1}^0 + \lambda_M f_M^0}{\tilde{\lambda}_{G1}^0} = \left(\frac{1}{\theta^0} \right)^{1/m_1} \frac{\lambda_{G1}^0 + \lambda_M f_M^0}{\lambda_{G1}^0} \,, \tag{B.14}$$

from which $\tilde{\lambda}_{G1}^0$ can be found, resulting $\tilde{\lambda}_{G1}^0 < \lambda_{G1}^0$ for $0.5 < \theta^0 < 1$. Since $\tilde{f}_M^0 = f_M^0$, from Eqs. $(B.11)$ we have $\tilde{f}_k^0 = f_k^0$, $k = m_1+1, \cdots, M-1$, so the property $(B.2)$ holds for $r=r_0$, and from (B.10) we have $\tilde{\lambda}_{G1}^0 \tilde{f}_{m_1}^0 = \lambda_{G1}^0 f_{m_1}^0$.

For $r > r_0$, we note that if

$$\tilde{\lambda}_{G1}(r) \tilde{f}_{m_1}(r) = \lambda_{G1}(r) f_{m_1}(r) \,, \tag{B.15}$$

then Eqs. $(B.5)$-$(B.7)$ have the solution $\tilde{f}_k(r) = f_k(r)$, $k = m_1+1, \cdots, M$ and thus $r\tilde{u}(r) = ru(r) = \lambda_M \int_{r_0}^{r} z f_M \, dz$. Setting $\tilde{\lambda}_{G1}(r) = \lambda_{G1}(r) f_{m_1}(r) / \tilde{f}_{m_1}(r)$ and substituting $u(r)$ to $\tilde{u}(r)$ into Eqs. $(B.3)$-$(B.4)$, we obtain the ODE system (with degeneracy at $r=r_0$)

$$u \frac{d\tilde{f}_1}{dr} = 2\lambda_M f_M - \lambda_{G1} f_{m_1} \frac{\tilde{f}_1}{\tilde{f}_{m_1}} - \lambda_M f_M \tilde{f}_1 \tag{B.16}$$

$$u \frac{d\tilde{f}_k}{dr} = \lambda_{G1} f_{m_1} \frac{\tilde{f}_{k-1}}{\tilde{f}_{m_1}} - \lambda_{G1} f_{m_1} \frac{\tilde{f}_k}{\tilde{f}_{m_1}} - \lambda_M f_M \tilde{f}_k \,, \quad k = 2, \cdots, m_1 \,. \tag{B.17}$$

The solution of the above system will give $\tilde{f}_{m_1}(r)$ from which $\tilde{\lambda}_{G1}(r)$ is found through $(B.15)$. It can be easily seen that the values $\tilde{f}_k^0$, $k = 1, \cdots, m_1$, obtained from $(B.8)$-$(B.11)$ when $\tilde{\lambda}_{G1}^0$ is

found from $(B.14)$ are the values at r_0 that can be deduced from $(B.16)$-$(B.17)$. Thus the value $\tilde{\lambda}_{G1}(r_0)$ obtained from the solution of $(B.16)$-$(B.17)$ is the value found from $(B.14)$.

References

[1] J. Folkman, Tumor angiogenesis. Adv. Cancer Res. 43 (1985) 175.

[2] W. Mueller-Klieser, Multicellular spheroids. A review on cellular aggregates in cancer research. J. Cancer Res. Clin. Oncol. 113 (1987) 101.

[3] J.A. Adam, General aspects of modeling tumor growth and immune response, in J.A. Adam, N. Bellomo (Eds.), A Survey of Models for Tumor-Immune System Dynamics, Birkhäuser, Boston, 1997, p. 187.

[4] J. Holash, P.C. Maisonpierre, D. Compton, P. Boland, C.R. Alexander, D. Zagzag, G.D. Yancopoulos, S.J. Wiegand, Vessel cooption, regression, and growth in tumors mediated by angiopoietins and VEGF. Science 284 (1999) 1994.

[5] G.D. Yancopoulos, S. Davis, N.W. Gale, J.S. Rudge, S.J. Wiegand, J. Holash, Vascular-specific growth factors and blood vessel formation. Nature 407 (2000) 242.

[6] I.F. Tannock, The relation between cell proliferation and the vascular system in a transplanted mouse mammary tumour. Br. J. Cancer 22 (1968) 258.

[7] D.G. Hirst, J. Denekamp, Tumour cell proliferation in relation to the vasculature. Cell Tissue Kinet. 12 (1979) 31.

[8] J.V. Moore, H.A. Hopkins, W.B. Looney, Tumour-cord parameters in two rat hepatomas that differ in their radiobiological oxygenation status. Radiat. Environ. Biophys. 23 (1984) 213.

[9] J.V. Moore, P.S. Hasleton, C.H. Buckley, Tumour cords in 52 human bronchial and cervical squamous cell carcinomas: Inferences for their cellular kinetics and radiobiology. Br. J. Cancer 51 (1985) 407.

[10] K.H. Falkvoll, The relationship between changes in tumour volume, tumour cell density and parenchymal cord radius in a human melanoma xenograft exposed to single dose irradiation. Acta Oncol. 29 (1990) 935.

[11] D.G. Hirst, V.K. Hirst, B. Joiner, V. Prise, K.M. Shaffi, Changes in tumour morphology with alterations in oxygen availability: further evidence for oxygen as a limiting substrate. Br. J. Cancer 64 (1991) 54.

[12] A. Bertuzzi, A. Fasano, A. Gandolfi, A mathematical model for the growth of tumor cords incorporating the dynamics of a nutrient, in: N. Kenmochi (Ed.), Free Boundary Problems: Theory and Applications. II, Gakkotosho, Tokyo, 2000, p. 31.

[13] A. Bertuzzi, A. Gandolfi, Cell kinetics in a tumour cord. J. theor. Biol. 204 (2000) 587.

[14] D.G. Kendall, On the role of variable cell generation time in the development of a stochastic birth process. Biometrika 35 (1948) 316.

[15] M. Takahashi, Theoretical basis for cell cycle analysis. I. Labelled mitosis wave method. J. Theor. Biol. 13 (1966) 202.

[16] M. Takahashi, Theoretical basis for cell cycle analysis. II. Further studies on labelled mitosis wave method. J. Theor. Biol. 18 (1968) 195.

[17] G.G. Steel, Growth Kinetics of Tumours: Cell Population Kinetics in Relation to the Growth and Treatment of Cancer, Clarendon Press, Oxford, 1977.

[18] J.M. Ortega, W.C. Rheinboldt, Iterative Solution of Nonlinear Equations in Several Variables, Academic Press, New York, 1970.